

Chemical characteristics of brown carbon in atmospheric particles at a suburban site near Guangzhou, China

Yi Ming Qin^{1,#}, Hao Bo Tan², Yong Jie Li³, Zhu Jie Li^{2,4}, Misha I. Schurman⁵, Li Liu^{2,6}, Cheng Wu⁷, and Chak K. Chan¹

¹School of Energy and Environment, City University of Hong Kong, Hong Kong, China

²Key Laboratory of Regional Numerical Weather Prediction, Institute of Tropical and Marine Meteorology, China Meteorological Administration, Guangzhou, China

³Department of Civil and Environmental Engineering, Faculty of Science and Technology, University of Macau, Macau, China

⁴School of Environmental Science and Engineering, Nanjing University of Information Science and Technology, Nanjing, China

1 ⁵ Zephyr Research Consultants, USA

⁶Department of Atmospheric Science, Sun yat-sen University, Guangzhou, China

⁷Institute of Mass Spectrometer and Atmospheric Environment, Jinan University, Guangzhou, China

now at School of Engineering and Applied Sciences, Harvard University, Cambridge, MA, USA

Correspondence to: Chak K. Chan (chak.k.chan@cityu.edu.hk) and Yong Jie Li (yongjieli@umac.mo)

Abstract:

Light-absorbing organic carbon (or brown carbon, BrC) in atmospheric particles has received much attention for its potential role in global radiative forcing. While a number of field measurement campaigns have differentiated light absorption by black carbon (BC) and BrC, the chemical characteristics of BrC are not well understood. In this study, we present co-located real-time light absorption and chemical composition measurements of atmospheric particles to explore the relationship between the chemical and optical characteristics of BrC at a suburban site downwind of Guangzhou, China from November to December 2014. BrC and BC contributions to light absorption were estimated using measurements from a seven-wavelength aethalometer, while the chemical composition of non-refractory PM₁ was measured with a high resolution time-of-flight aerosol mass spectrometer (HR-ToF-AMS). Using the Absorption Angstrom Exponent (AAE) method, we estimated that BrC contributed 23.6% to the total aerosol absorption at 370 nm, 18.1% at 470 nm, 10.7% at 520 nm, 10.7% at 590 nm, and 10.5% at 660 nm. Biomass burning organic aerosol (BBOA) has the highest mass absorption coefficient among sources of organic aerosols. Its contribution to total brown carbon absorption coefficient decreased but that of low-volatility oxygenated organic aerosol (LVOOA) increased with increasing wavelength, suggesting the need for wavelength-dependent light absorption analysis for BrC in association with its chemical makeup. Clear correlations of N-containing ion fragments with absorption coefficient were observed. These correlations also depended on their degrees of unsaturation/cyclization and oxygenation. While the current study relates light absorption by BrC to ion fragments, more detailed chemical characterization is warranted to constrain this relationship.

3 Introduction:

4 Atmospheric particles participate considerably in the global climate direct effect via their light-
5 scattering (e.g., sulfate) and/or light-absorbing components (e.g., black carbon, BC). BC is major
6 contributor to light absorption that leads to positive radiative forcing, increasing the average
7 temperature of the atmosphere. The BrC absorption contribution to total aerosol light absorption
8 can reach 20–50% over regions dominated by seasonal biomass burning and biofuel combustion
9 (Feng et al., 2013). A significant difference in optical feature of BrC and BC is that BrC absorbs
10 light primarily at UV and short-visible wavelengths with the absorption decreasing significantly
11 at long wavelengths, while BC absorbs strongly and constantly throughout the UV to visible
12 spectrum (Andreae and Gelencsér, 2006; Bergstrom et al., 2007; Bond and Bergstrom, 2006). In
13 global climate models, the direct radiative forcing of organic aerosols at the top of atmosphere can
14 shift from cooling (-0.08 Wm^{-2}) to warming ($+0.025 \text{ Wm}^{-2}$) when strong BrC absorption is
15 included (Feng et al., 2013). However, uncertainties in the sources, formation, chemical
16 composition, and absorption properties of BrC hinder more accurate estimations of radiative
17 forcing induced by atmospheric particles.

18 BrC is operationally defined and has many chemical constituents, which makes chemical
19 characterization quite challenging. Both primary and secondary organic aerosols can act as BrC
20 (Laskin et al., 2015). For example, biomass burning organic aerosol (BBOA) has been identified
21 as a contributor to BrC in rural areas in the southern United States, while coal combustion organic
22 aerosol (CCOA) contributes substantially to BrC during winter in Beijing (Yan et al., 2017).
23 Species from secondary formation processes, such as humic-like substances (HULIS) formed by
24 in-cloud processing (Rinco et al., 2009), species from gas-phase photo-oxidation of volatile
25 organic compounds (VOCs) in the presence of NO_x , and species from reactions between carbonyl
26 compounds and ammonia in the aqueous film at the particle surface, can also contribute to BrC
27 (Gen et al., 2018; Laskin et al., 2010; Liu et al., 2015). Highly conjugated organics, nitro-aromatic
28 compounds, imidazoles, and other N-heterocyclic compounds have been found in BrC (Laskin et
29 al., 2015; Lin et al., 2016). Sun et al. (2007) also found that light-absorbing organic molecules in
30 BrC are likely large (i.e., possessing > 18 carbon atoms); these molecules are generally highly
31 unsaturated and contain three or more oxygen atoms and/or one or more nitrogen atoms.

32 The Pearl River Delta (PRD) region, one of the most economically developed regions in China,
33 suffers under air pollution from a variety of sources (Chan and Yao, 2008; Li et al., 2017). Source

34 apportionment using positive matrix factorization (PMF) analysis of mass spectral data sets from
35 high resolution time-of-flight aerosol mass spectrometry (HR-ToF-AMS) has revealed that the
36 organic aerosol (OA) in this region arises from traffic emissions (i.e., hydrocarbon-like organic
37 aerosol, or HOA), biomass burning (BBOA), cooking (COA), and secondary formation (i.e.,
38 oxygenated organic aerosols, or OOAs). In the PRD, HOA is often the largest contributor to OA
39 at urban sites (He et al., 2011), while SOA plays a more important role at rural sites (Gong et al.,
40 2012; Huang et al., 2011). BBOA has also been found to contribute significantly to total OA in the
41 PRD region, with contributions of 24% at an urban site in Shenzhen (He et al., 2011) and 14% and
42 25% at rural sites in Heshan and Kaiping, respectively (Gong et al., 2012; Huang et al., 2011).
43 Yuan et al. (2016) attributed 6-12% of the total aerosol absorption at 405 nm at a rural site in the
44 PRD to BrC; the authors found higher BrC contributions during fall, which they ascribed to
45 biomass burning (BBOA) activities nearby. However, the BrC components responsible for light
46 absorption remain relatively unknown; this hinders a thorough understanding of the relationships
47 between optical properties and chemical characteristics and, in turn, the realization of a generalized
48 framework that can be extended to other sources and regions.

49 In this work, we present simultaneous measurements of aerosol chemical composition and light
50 absorption of aerosol particles at a suburban site downwind of Guangzhou in the PRD, China.
51 Contributions of BC and BrC to total aerosol light absorption were differentiated and quantified
52 using measurements from a seven-wavelength aethalometer. Sources of OA, which were
53 determined using PMF analysis, were correlated to BrC light absorption to identify the major
54 contributor(s) to short-wavelength light absorption. More detailed chemical characteristics, such
55 as N-containing ion fragments, the degree of unsaturation (indicated by the ion double bond
56 equivalent, or ion DBE), and the degree of oxygenation (indicated by the number of oxygen atoms
57 in ions), were also used to investigate the structural characteristics of BrC related to light
58 absorption.

59 Methodology

60 1. Sampling site

61 We conducted field measurements at the Guangzhou Panyu Atmospheric Composition Station
62 (GPACS, 23°00' N, 113°21' E), on the periphery of Guangzhou, China, from November 7, 2014

63 to January 3, 2015. The GPACS is located on top of a hill with an altitude of approximately 150
64 m a.s.l. (Cheung et al., 2016; Tan et al., 2013; Zou et al., 2015); it is approximately 15 km south
65 of the city center and was downwind of the central city throughout the sampling period, during
66 which north winds prevailed (Qin et al., 2017).

67 2. Measurements and data analysis

68 Aerosol light absorption was measured with a seven-wavelength aethalometer (Magee Scientific,
69 model AE33) at 370, 470, 520, 590, 660, 880, and 950 nm. Ambient air was drawn through a 2.5-
70 μm cut-off inlet at 2 L/min before entering the aethalometer; particles were collected on the filter
71 substrate, and light attenuation at the wavelengths above was recorded continuously. A diffusion
72 drier was used to dry the sampled air stream, which reduced the RH of the air to below 30 %. The
73 optical properties of the collected particles were determined by comparing light attenuation in
74 particle-laden and particle-free filter areas (Weingartner et al., 2003). To convert aerosol particles
75 light attenuation coefficients at the filter substrate to the light absorption coefficients suspended in
76 the air, a real-time compensation parameter k and a fixed multiple scattering parameter C were
77 used. The real-time loading effect correction was performed using two parallel measurements of
78 optical attenuations at different accumulation rates. $C_{ref}=2.14$ for quartz filter and $C_{ref}=1.57$ for
79 tetrafluoroethylene (TFE)-coated glass filter were recommended from previously studies for the
80 fresh soot particles (Drinovec et al., 2015; Weingartner et al., 2003). However, with the presence
81 of semi-volatile oxidation products, significantly higher values ($C=3.6\pm 0.6$) were observed in the
82 organic coating experiment using a quartz filter (Weingartner et al., 2003). Wavelength
83 dependence of C has also been reported in the literature (Arnott et al., 2005; Schmid et al., 2006;
84 Segura et al., 2014) . A broad range of C (from 2.8 to 7.8) at several sites was also used by Collaud
85 Coen et al. (2010). As the multiple scattering parameter (C) may be site specific, we further
86 compared the absorption from AE33 with cavity ring-down spectroscopy (CRD, Hexin XG-1000)
87 and Nephelometer (TSI, 3563). The nephelometer was calibrated by CO_2 weekly during the field
88 campaign. Particle-free air was checked once a day. The CRD was calibrated using polystyrene
89 spheres with known indices of refraction before the campaign. We extracted the light absorption
90 based on extinction and scattering measurements from cavity ring-down spectroscopy and
91 Nephelometer, respectively, as below.

$$92 \quad b_{abs} = \sigma_{ext} - \sigma_{sp} \quad (1)$$

93 where b_{abs} , σ_{ext} and σ_{sp} are absorption coefficient, extinction coefficient and scattering
94 coefficient.

95 The scatter plot of absorption at 532 nm from measurement from the aethalometer (AE33) and that
96 calculated from CRD and Nephelometer (CRD-Neph) is displayed in Figure 1. AE 33 absorption
97 coefficient was higher than the absorption estimated from Eq. 1. by a factor of 2.10. Therefore, the
98 final multiple scattering parameter (C) was set to $C_{final} = C_{ref} \times 2.10 = 3.29$. This value is
99 comparable with previous aethalometer measurements (C=3.48) in the PRD region (Wu et al.,
100 2009, 2013).

101 The non-refractory chemical composition of submicron aerosols was measured with an Aerodyne
102 HR-ToF-AMS (Aerodyne Research Inc., Billerica, MA, USA). Briefly, the AMS collected five-
103 minute-average particle mass spectra for the high-sensitivity V plus particle time-of-flight (PToF)
104 mode and the high-resolution W mode. AMS data analysis was performed using the SQUIRREL
105 (v1.56D) and PIKA (v1.15D) toolkits in Igor Pro (WaveMetrics Inc., Lake Oswego, OR). Source
106 apportionment was performed via PMF analysis with Multilinear Engine 2 (ME-2) via the SoFi
107 interface (Canonaco et al., 2013). Five factors, including HOA, COA, BBOA, semi-volatile
108 oxygenated organic aerosol (SVOOA), and low-volatility oxygenated organic aerosol (LVOOA),
109 were resolved (Qin et al., 2017). The campaign average OA composition was dominated by
110 surrogates of SOA (SVOOA + LVOOA). However, freshly-emitted hydrocarbon-like organic
111 aerosols (HOA) contributed up to 40.0% of OA during high-OA periods; during nighttime, HOA
112 contributed 23.8% to 28.4% on average. BBOA contributed 9.6% ($1.87 \mu\text{g}/\text{m}^3$) of total OA in
113 November and 6.5% ($1.38 \mu\text{g}/\text{m}^3$) in December. AMS data treatment was discussed in detail in
114 Qin et al. (2017). Data from a thermo-optical elemental carbon and organic carbon (ECOC)
115 analyzer (Sunset Laboratory Inc.) were also used for comparison.

116 Results and discussion

117 1. Aerosol absorption

118 Figure 2a shows the box-whisker plot of aerosol absorption coefficients (b_{abs}) from 370 nm to 950
119 nm from the aethalometer measurements during the campaign. The campaign-average absorption
120 coefficients were 56.00 Mm^{-1} at 370 nm, 40.99 Mm^{-1} at 470 nm, 34.76 Mm^{-1} at 520 nm, 29.91
121 Mm^{-1} at 590 nm, 26.69 Mm^{-1} at 660 nm, 18.06 Mm^{-1} at 880 nm, and 16.71 Mm^{-1} at 950 nm.

122 In multi-wavelength absorption measurements, the total absorption Ångström exponent (AAE) can
 123 be calculated by a power-law fitting of the absorption coefficient over all available wavelengths.
 124 AAE of unity has been widely used for pure black carbon, while a shift to higher AAE value has
 125 been observed with the presence of brown carbon. The reason behind is that BrC has a much
 126 stronger absorption at UV and short visible wavelengths than at long visible wavelengths, which
 127 yields a steeper curve (Andreae and Gelencsér, 2006; Bergstrom et al., 2007; Bond and Bergstrom,
 128 2006). The presence of non-absorbing OA shells over BC cores may also lead to a shift of AAE
 129 (Gyawali et al., 2009). This latter possibility is analyzed in a separated manuscript (Li et al., in
 130 preparation). Briefly, a Mie theory model was used to estimate the AAE for BC-containing
 131 particles (AAE_{BC}) at core-shell scenarios with different refractive indexes. AAE_{BC} is sensitive to
 132 specific refractive index of core and shell of the particles and the size of the particle. The size
 133 distribution is from scanning mobility particle sizer and aerodynamic particle sizer measurement,
 134 and we vary the refractive index of the core and shell in the model. The method is adopted from
 135 Tan et al. (2016) . In general, AAE_{BC} increases as the real part refractive index of the core
 136 increases or the imaginary decreases, or alternatively real part of the shell increases. The AAE_{BC}
 137 ranges from 0.67-1.03 across the different scenario (Table S1). As shown in Figure 2b, the AAE
 138 values, which average at 1.43, are almost always higher than 1, indicating appreciable
 139 contributions from BrC to particle light absorption at this site.

140
 141 To further explore the importance of BrC at this site, BrC absorption at a short wavelength λ_1
 142 (b_{BrC,λ_1}) can be derived by subtracting BC absorption (b_{BC,λ_1}) from the total aerosol absorption
 143 (Lack and Langridge, 2013) via:

$$144 \quad b_{BrC,\lambda_1} = b_{\lambda_1} - b_{BC,\lambda_1} \quad (2)$$

145 where absorption b_{λ_1} is the measured absorption at the short wavelength λ_1 . BC absorption at λ_1
 146 (b_{BC,λ_1}) can be obtained from the AAE value of BC (AAE_{BC}) via:

$$147 \quad b_{BC,\lambda_1} = b_{\lambda_2} \times (\lambda_2 / \lambda_1)^{AAE_{BC}} \quad (3)$$

149 where b_{λ_2} is the absorption at a longer wavelength λ_2 (880 nm), which is assumed to have no
 150 contributions from BrC or dust (Drinovec et al., 2015; Zhu et al., 2017). The uncertainty involved
 151 in attributing BrC and BC absorption at short wavelengths has been explored explicitly by Lack

152 and Langridge (2013). This uncertainty is primarily from uncertainty of choice of AAE_{BC} . Based
153 on the AAE_{BC} from Mie theory model, a sensitivity analysis of BrC contribution to total light
154 absorption is presented in Figure S1.

155 Figure 3 shows the b_{abs} attributed to BC and BrC (b_{BC} and b_{BrC}) at different wavelengths. Aerosol
156 light absorption coefficients were dominated by BC, but b_{BrC} was not negligible, especially at short
157 wavelengths. The campaign-average b_{BrC} values were 13.67, 7.56, 4.49, 3.22, and 2.81 Mm^{-1} at
158 370, 470, 520, 590, and 660 nm, respectively; BrC absorption contributed 23.6%, 18.1%, 10.7%,
159 10.7%, and 10.5% of the total absorption at the corresponding wavelengths. The proportions of
160 BrC and BC in our campaign were slightly higher than those reported an earlier study in the PRD
161 by Yuan et al. (2016). In their study, the average light absorption contributions of BrC during
162 Shenzhen winter, Shenzhen fall, and Heshan fall campaigns were 11.7%, 6.3%, and 12.1% at 405
163 nm and 10.0%, 4.1%, and 5.5% at 532 nm, respectively.

164 Figure 4 shows the diurnal variations of both b_{BrC} and b_{BC} at 370, 470, 520, 590, and 660 nm,
165 respectively. In general, the diurnal cycles of b_{BrC} and b_{BC} share similar patterns, indicating that
166 they may have similar sources. However, it should be noted that some OA factors, such as BBOA
167 and HOA, also share similar patterns(Qin et al., 2017). Overall, there were two peaks at each
168 wavelength. The first peak appeared in the morning at around 8:00 LT, with a peak before 8:00
169 LT for longer wavelength and after 8:00 LT for shorter wavelength. The second peak appeared at
170 21:00 LT and its intensity decreased until 24:00 LT. These changes may be attributed to diurnal
171 changes in BrC sources, which most likely originated from crop residual burning in fall and winter
172 in nearby regions (Wang et al., 2017). The diurnal variations of the different wavelengths were not
173 significantly different, although short wavelengths exhibited more obvious diurnal variations.

174

175 2. Correlation of light absorption by BrC with OA components

176 To explore the possible sources of BrC, correlations were determined between b_{BrC} at 370 nm
177 ($b_{BrC,370}$) and various OA types. Data at 370 nm were chosen (over data at longer wavelengths) for
178 their higher signal-to-noise ratios and larger contributions of BrC to light absorption. Figure 5
179 shows that BBOA concentrations and $b_{BrC,370}$ were well correlated (Pearson's correlation
180 coefficient, $R_p = 0.58$). More interestingly, a moderate correlation ($R_p = 0.40$) was also found
181 between $b_{BrC,370}$ and the LVOOA mass concentration. Although the LVOOA factor was not further
182 resolved into OOA factors with biomass origins, it is likely that a portion of LVOOA was formed

183 from biomass burning precursors through either gas-phase oxidation or heterogeneous reactions.
184 Satish et al. (2017) found correlations between BrC absorption and both primary BBOA and
185 BBOA-related SVOOA factors. They also reported that the slope of the correlation between
186 $b_{BrC,370}$ and BBOA (slope = 1.35) was 4.8 times higher than that between $b_{brc,370}$ and one of the
187 biomass burning SVOOA factors (slope = 0.28), indicating that aging may have reduced the
188 absorption capacity of biomass-related OA.

189 Multiple regression analysis was also used to resolve the correlation factors of each OA component
190 ($\text{m}^2 \text{g}^{-1}$) at each wavelength.

$$191 \quad b_{BrC} = a*[\text{HOA}] + b*[\text{COA}] + c*[\text{BBOA}] + d*[\text{SVOOA}] + e*[\text{LVOOA}] \quad (4)$$

192 where a, b, c, d, e indicates the correlation factors of each OA component ($\text{m}^2 \text{g}^{-1}$) and [...] indicates
193 the mass concentration of each OA component. These correlation factors obtained are equivalent
194 to MAC mass absorption coefficient (MAC) of each OA component. We will use these factors to
195 compare with MAC reported in the literature later.

196 Washenfelder et al. (2015) reported a MAC of $1.3 \pm 0.06 \text{ m}^2 \text{g}^{-1}$ using the b_{BrC} at 365 nm for
197 BBOA in the rural southeastern United States, which was 40 to 135 times higher than the MAC
198 values reported for other OA factors. Di Lorenzo et al. (2017) found that both BBOA and more-
199 oxidized oxygenated organic aerosol (MO-OOA) were associated with water soluble BrC and that
200 the MAC of BBOA doubled that of MO-OOA. However, Forrister et al. (2015) observed that BrC
201 in wildfire plumes had a lifetime of roughly 9 to 15 hours, probably due to conversion to SOA
202 with lower light absorption capacity. In our study, the MAC (correlation factor in Table 1) of
203 BBOA at 370 nm was $3.4 \pm 0.41 \text{ m}^2 \text{g}^{-1}$, roughly 3.4 times that of LVOOA ($1.04 \pm 0.08 \text{ m}^2 \text{g}^{-1}$).
204 Like the studies listed above (Forrister et al., 2015; Di Lorenzo et al., 2017; Washenfelder et al.,
205 2015), our results suggest that the absorption coefficient of nascent BBOA is higher than that of
206 its aged counterpart at short wavelength. However, it should be noted that LVOOA might consist
207 of some other non-absorbing SOA components with no biomass origin. It is therefore important to
208 consider chromophore lifetimes when modeling light absorption by BrC. As noted in Laskin et al.
209 (2015), the physicochemical properties of chromophores in BrC may exhibit dynamic changes that
210 are not yet sufficiently understood. In addition, the difference between MAC values of BBOA and
211 LVOOA decreased for longer wavelengths. The MAC values of BBOA were roughly 3.4, 1.8, 1.5,
212 1.48, and 0.80 times those of LVOOA at 370, 470, 520, 570, and 660 nm, respectively. The

213 contribution to total absorption coefficient also varied with wavelengths. The contribution from
214 BBOA decrease from 25.8% to 10.1% from 370 nm to 660 nm, while the contribution from
215 LVOOA increase from 49.3% to 60.2 % from 370nm to 660nm. The contribution of HOA was
216 more stable across different wavelengths but was also significant, likely due to the high mass
217 concentration of HOA. The exponential decay of b_{abs} for different light-absorbing components was
218 shown in Figure 7. The fitted AAE values for those components are 3.52, 3.28, 5.50 and 2.67 for
219 total BrC, HOA, BBOA and LVOOA respectively. These results indicate that variability of AAE
220 values ranging from different sources which is likely inherent to the chemical variability of BrC
221 constituents. Altogether, these observations indicate that the wavelength-dependent light
222 absorption of different OAs must be considered in light absorption models.

223 3. Correlation of b_{BrC} with N-containing organic ions

224 The chromophores in BrC that are responsible for OA light absorption are not well characterized.
225 Structurally, light absorption depends on the extent of sp^2 hybridization, in which π electrons are
226 usually found (Bond and Bergstrom, 2006). Of the elements commonly found in OA, both C and
227 N have strong tendencies toward sp^2 hybridization. It has also been found that, despite their small
228 OA mass fraction contributions, N-containing organic species in OA can be responsible for
229 appreciable light absorption (Chen et al., 2016; Laskin et al., 2015). Thus, we examined the
230 correlations between b_{BrC} and N-containing ions from AMS measurements. These ion fragments,
231 including the $C_xH_yN^+$ and $C_xH_yO_zN^+$ families, likely originated from N-heterocyclic compounds.
232 Figure 6 shows that the mass loadings of $C_xH_yN^+$ and $C_xH_yO_zN^{++}$ families are correlated with b_{BrC}
233 at 370 nm and that correlations are stronger for fragments containing both N and O atoms. These
234 results are consistent with Chen et al. (2016), who suggested that organic compounds with O and
235 N atoms might contribute substantially to total light absorption and fluorescence in OA
236 components.

237 The effects of oxygenation (as indicated by the number of O atoms in an ion) and
238 unsaturation/cyclization (as indicated by the ion double bond equivalent, or ion DBE) were also
239 examined for each $C_xH_yN^+$ and $C_xH_yO_zN^+$ ion family. Several studies found that species with high
240 DBE values may have substantial network of conjugated double bonds and likely contribute to
241 light absorption (Budisulistiorini et al., 2017; Laskin et al., 2014; Lin et al., 2016). The ion DBE

242 represents the number of double bonds (unsaturation) or rings (cyclization) that an ion contains
243 and is calculated on the basis of the elemental formula via the following equation:

$$244 \quad \text{DBE} = C + 1 - H/2 - X/2 + N/2 \quad (4)$$

245 where C, H, X, and N are the number of carbon, hydrogen, halogen (Cl, Br, I, and F), and nitrogen
246 atoms present in the ion, respectively.

247 Figure 8a shows the correlation coefficients between b_{BrC} at all available wavelengths and the
248 mass loadings of each ion in $C_xH_yN^+$ and $C_xH_yNO_z^+$ families at different DBE values. For the
249 $C_xH_yN^+$ family, R_p increased as DBE increased across all wavelength, suggesting that b_{BrC} was
250 better correlated with fragments with higher degrees of unsaturation or cyclization. And increasing
251 trend of R_p as DBE increased is more obvious for short wavelengths (e.g. λ at 370 nm and 470
252 nm), suggesting that the absorption at short wavelengths are more associated with the unsaturation
253 or cyclization. Indeed, in saturated organics, light absorption involves excitation of n electrons,
254 which requires more energy and, therefore, shorter incident wavelengths (e.g., short UV). In
255 unsaturated organics, the delocalized π electrons are in clusters of sp^2 hybrid bonds and in longer
256 conjugated systems, such that the energy difference between the excited state and the ground
257 state goes down, which makes the absorption band shift to longer wavelengths. These structural
258 features may explain in part the increased correlation between mass loadings of the $C_xH_yN^+$ family
259 and light absorption with decreasing ion saturation. For the $C_xH_yNO_z^+$ family, we did not observe
260 obvious trends in the correlation coefficient with changing degree of saturation/cyclization (Figure
261 8b). This phenomenon is consistent across different wavelength. However, the overall Pearson's
262 R_s of b_{BrC} with $C_xH_yNO_z^+$ were higher than those with $C_xH_yN^+$. The R_p for each group of ions is
263 higher at short wavelengths (λ at 370 nm and 470 nm).

264 Conclusions

265 This paper presents collocated, real-time atmospheric particle light absorption and chemical
266 composition measurements at a suburban site in PRD, China. While BC dominated aerosol light
267 absorption, BrC also contributed to absorption at short wavelengths. The aerosol light absorption
268 coefficients of BrC were 13.67, 7.56, 4.49, 3.22, and 2.81 Mm^{-1} at 370, 470, 520, 590, and 660 nm,
269 respectively, and BrC contributed 23.6%, 18.1%, 10.7%, 10.7%, and 10.5% of the total absorption
270 at the corresponding wavelengths. Hydrocarbon-like organic aerosol (HOA), biomass burning

271 organic aerosol (BBOA) and low-volatility oxygenated organic aerosol (LVOOA) were also
272 substantial for the source of BrC. At short wavelength (370 nm), the mass absorption coefficient
273 of BBOA was higher than those of HOA and LVOOA. However, the difference between the mass
274 absorption coefficients of BBOA and other OA factors decreased with increasing wavelength. The
275 contribution of different OA sources to total absorption coefficient also varied with wavelengths.
276 Such a wavelength dependent trend is also observed for their contribution to total BrC absorption
277 coefficients. $C_xH_yN^+$ and $C_xH_yO_zN^+$, were likely the chromophores responsible for the observed
278 BrC light absorption. The mass loadings of $C_xH_yN^+$ and $C_xH_yO_zN^+$ ion families became better
279 correlated with the BrC light absorption coefficient as their degrees of unsaturation/cyclization and
280 oxygenation increased. This study shows wavelength-dependent light absorption by BrC is
281 strongly influenced by moderately specific molecular characteristics such as degrees of
282 unsaturation/ cyclization and oxygenation. An exploration of the absorptive properties of more
283 specific molecular features, such as the chemical identities of BrC constituents, would require a
284 more detailed chemical characterization of the highly complex OA composition.

285

286 Acknowledgements

287 This work was supported by the National Key Project of the Ministry of Science and Technology
288 of the People's Republic of China (2016YFC0201901, 2016YFC0203305). The authors would
289 like to acknowledge Hong Kong University of Science and Technology for the use of their AMS.
290 We also thank Jianhuai Ye for fruitful discussion. Chak K. Chan would like to acknowledge the
291 Science Technology and Innovation Committee of Shenzhen municipality (project no. 41675117).
292 Yong Jie Li gratefully acknowledges support from Science and Technology Development Fund of
293 Macau (FDCT-136/2016/A3).

294

295

296 References

- 297 Andreae, M. O. and Gelencsér, A.: Black carbon or brown carbon? The nature of light-absorbing
298 carbonaceous aerosols, *Atmos. Chem. Phys.*, 6(3), 3419–3463, doi:10.5194/acpd-6-3419-2006,
299 2006.
- 300 Arnott, W. P., Hamasha, K., Moosmüller, H., Sheridan, P. J. and Ogren, J. A.: Towards aerosol
301 light-absorption measurements with a 7-wavelength aethalometer: Evaluation with a
302 photoacoustic instrument and 3-wavelength nephelometer, *Aerosol Sci. Technol.*, 39(1), 17–29,
303 doi:10.1080/027868290901972, 2005.
- 304 Bergstrom, R. W., Pilewskie, P., Russell, P. B., Redemann, J., Bond, T. C., Quinn, P. K. and
305 Sierau, B.: Spectral absorption properties of atmospheric aerosols, *Atmos. Chem. Phys.*, 7(23),
306 5937–5943, doi:10.5194/acp-7-5937-2007, 2007.
- 307 Bond, T. C. and Bergstrom, R. W.: Light Absorption by Carbonaceous Particles: An
308 Investigative Review, *Aerosol Sci. Technol.*, 40(1), 27–67, doi:10.1080/02786820500421521,
309 2006.
- 310 Budisulistiorini, S. H., Riva, M., Williams, M., Chen, J., Itoh, M., Surratt, J. D. and Kuwata, M.:
311 Light-Absorbing Brown Carbon Aerosol Constituents from Combustion of Indonesian Peat and
312 Biomass, *Environ. Sci. Technol.*, 51(8), 4415–4423, doi:10.1021/acs.est.7b00397, 2017.
- 313 Canonaco, F., Crippa, M., Slowik, J. G., Baltensperger, U. and Prévôt, A. S. H.: SoFi, an IGOR-
314 based interface for the efficient use of the generalized multilinear engine (ME-2) for the source
315 apportionment: ME-2 application to aerosol mass spectrometer data, *Atmos. Meas. Tech.*, 6(12),
316 3649–3661, doi:10.5194/amt-6-3649-2013, 2013.
- 317 Chan, C. K. and Yao, X.: Air pollution in mega cities in China, *Atmos. Environ.*, 42(1), 1–42,
318 doi:10.1016/j.atmosenv.2007.09.003, 2008.
- 319 Chen, Q., Ikemori, F. and Mochida, M.: Light Absorption and Excitation-Emission Fluorescence
320 of Urban Organic Aerosol Components and Their Relationship to Chemical Structure, *Environ.*
321 *Sci. Technol.*, 50(20), 10859–10868, doi:10.1021/acs.est.6b02541, 2016.
- 322 Cheung, H. H. Y., Tan, H., Xu, H., Li, F., Wu, C., Yu, J. Z. and Chan, C. K.: Measurements of
323 non-volatile aerosols with a VTDMA and their correlations with carbonaceous aerosols in
324 Guangzhou, China, *Atmos. Chem. Phys.*, 16(13), 8431–8446, doi:10.5194/acp-16-8431-2016,
325 2016.
- 326 Collaud Coen, M., Weingartner, E., Apituley, A., Ceburnis, D., Fierz-Schmidhauser, R., Flentje,
327 H., Henzing, J. S., Jennings, S. G., Moerman, M., Petzold, A., Schmid, O. and Baltensperger, U.:
328 Minimizing light absorption measurement artifacts of the Aethalometer: Evaluation of five
329 correction algorithms, *Atmos. Meas. Tech.*, 3(2), 457–474, doi:10.5194/amt-3-457-2010, 2010.
- 330 Drinovec, L., Močnik, G., Zotter, P., Prévôt, A. S. H., Ruckstuhl, C., Coz, E., Rupakheti, M.,
331 Sciare, J., Müller, T., Wiedensohler, A. and Hansen, A. D. A.: The “dual-spot” Aethalometer: An
332 improved measurement of aerosol black carbon with real-time loading compensation, *Atmos.*
333 *Meas. Tech.*, 8(5), 1965–1979, doi:10.5194/amt-8-1965-2015, 2015.
- 334 Feng, Y., Ramanathan, V. and Kotamarthi, V. R.: Brown carbon: A significant atmospheric

335 absorber of solar radiation, *Atmos. Chem. Phys.*, 13(17), 8607–8621, doi:10.5194/acp-13-8607-
336 2013, 2013.

337 Forrister, H., Liu, J., Scheuer, E., Dibb, J., Ziemba, L., Thornhill, K. L., Anderson, B., Diskin,
338 G., Perring, A. E., Schwarz, J. P., Campuzano-Jost, P., Day, D. A., Palm, B. B., Jimenez, J. L.,
339 Nenes, A. and Weber, R. J.: Evolution of brown carbon in wildfire plumes, *Geophys. Res. Lett.*,
340 42(11), 4623–4630, doi:10.1002/2015GL063897, 2015.

341 Gen, M., Huang, D. and Chan, C. K.: Reactive uptake of glyoxal by ammonium containing salt
342 particles as a function of relative humidity, *Environ. Sci. Technol.*, 52, 6903–6911,
343 doi:10.1021/acs.est.8b00606, 2018.

344 Gong, Z., Lan, Z., Xue, L., Zeng, L., He, L. and Huang, X.: Characterization of submicron
345 aerosols in the urban outflow of the central Pearl River Delta region of China, *Front. Environ.*
346 *Sci. Eng. China*, 6(5), 725–733, doi:10.1007/s11783-012-0441-8, 2012.

347 Gyawali, M., Arnott, W. P., Lewis, K. and Moosmüller, H.: In situ aerosol optics in Reno, NV,
348 USA during and after the summer 2008 California wildfires and the influence of aerosol
349 coatings, *Atmos. Chem. Phys. Discuss.*, 9, 8007–8015, doi:10.5194/acp-9-8007-2009, 2009.

350 He, L.-Y., Huang, X.-F., Xue, L., Hu, M., Lin, Y., Zheng, J., Zhang, R. and Zhang, Y.-H.:
351 Submicron aerosol analysis and organic source apportionment in an urban atmosphere in Pearl
352 River Delta of China using high-resolution aerosol mass spectrometry, *J. Geophys. Res.*,
353 116(D12), D12304, doi:10.1029/2010JD014566, 2011.

354 Huang, X.-F. F., He, L.-Y. Y., Hu, M., Canagaratna, M. R., Kroll, J. H., Ng, N. L., Zhang, Y.-H.
355 H., Lin, Y., Xue, L., Sun, T.-L. L., Liu, X.-G. G., Shao, M., Jayne, J. T. and Worsnop, D. R.:
356 Characterization of submicron aerosols at a rural site in Pearl River Delta of China using an
357 Aerodyne High-Resolution Aerosol Mass Spectrometer, *Atmos. Chem. Phys.*, 11(5), 1865–1877,
358 doi:10.5194/acp-11-1865-2011, 2011.

359 Lack, D. A. and Langridge, J. M.: On the attribution of black and brown carbon light absorption
360 using the angstrom exponent, *Atmos. Chem. Phys.*, 13(20), 10535–10543, doi:10.5194/acp-13-
361 10535-2013, 2013.

362 Laskin, A., Laskin, J. and Nizkorodov, S. a.: Chemistry of Atmospheric Brown Carbon, *Chem.*
363 *Rev.*, 115(10), 4335–4382, doi:10.1021/cr5006167, 2015.

364 Laskin, J., Laskin, A., Roach, P. J., Slysz, G. W., Anderson, G. A., Nizkorodov, S. A., Bones, D.
365 L. and Nguyen, L. Q.: Mass Spectrometry for Chemical Characterization of Organic Aerosols, ,
366 82(5), 2048–2058, doi:10.1029/2007JD008683, 2010.

367 Laskin, J., Laskin, A., Nizkorodov, S. A., Roach, P., Eckert, P., Gilles, M. K., Wang, B., Lee, H.
368 J. and Hu, Q.: Molecular selectivity of brown carbon chromophores, *Environ. Sci. Technol.*,
369 48(20), 12047–12055, doi:10.1021/es503432r, 2014.

370 Li, Y. J., Sun, Y., Zhang, Q., Li, X., Li, M., Zhou, Z. and Chan, C. K.: Real-time chemical
371 characterization of atmospheric particulate matter in China : A review, *Atmos. Environ.*, 158,
372 270–304, doi:10.1016/j.atmosenv.2017.02.027, 2017.

373 Lin, P., Aiona, P. K., Li, Y., Shiraiwa, M., Laskin, J., Nizkorodov, S. A. and Laskin, A.:
374 Molecular Characterization of Brown Carbon in Biomass Burning Aerosol Particles, *Environ.*

375 Sci. Technol., 50(21), 11815–11824, doi:10.1021/acs.est.6b03024, 2016.

376 Liu, P. F., Abdelmalki, N., Hung, H. M., Wang, Y., Brune, W. H. and Martin, S. T.: Ultraviolet
377 and visible complex refractive indices of secondary organic material produced by photooxidation
378 of the aromatic compounds toluene and m-xylene, *Atmos. Chem. Phys.*, 15(3), 1435–1446,
379 doi:10.5194/acp-15-1435-2015, 2015.

380 Di Lorenzo, R. A., Washenfelder, R. A., Attwood, A. R., Guo, H., Xu, L., Ng, N. L., Weber, R.
381 J., Baumann, K., Edgerton, E. and Young, C. J.: Molecular-Size-Separated Brown Carbon
382 Absorption for Biomass-Burning Aerosol at Multiple Field Sites, *Environ. Sci. Technol.*, 51(6),
383 3128–3137, doi:10.1021/acs.est.6b06160, 2017.

384 Massabo, D., Caponi, L., Bernardoni, V., Bove, M. C., Brotto, P., Calzolari, G., Cassola, F.,
385 Chiari, M., Fedi, M. E., Fermo, P., Giannoni, M., Lucarelli, F., Nava, S., Piazzalunga, A., Valli,
386 G., Vecchi, R. and Prati, P.: Multi-wavelength optical determination of black and brown carbon
387 in atmospheric aerosols, *Atmos. Environ.*, 108, 1–12, doi:10.1016/j.atmosenv.2015.02.058,
388 2015.

389 Qin, Y. M., Tan, H. B., Li, Y. J., Schurman, M. I., Li, F., Canonaco, F., Prévôt, A. S. H. and
390 Chan, C. K.: Impacts of traffic emissions on atmospheric particulate nitrate and organics at a
391 downwind site on the periphery of Guangzhou, China, *Atmos. Chem. Phys.*, 2017(x), 1–31,
392 doi:10.5194/acp-2017-116, 2017.

393 Rinco, A. G., Guzman, M. I., Hoffmann, M. R. and Colussi, A. J.: Optical Absorptivity versus
394 Molecular Composition of Model Organic Aerosol Matter, , 10512–10520, 2009.

395 Satish, R., Shamjad, P., Thamban, N., Tripathi, S. and Rastogi, N.: Temporal Characteristics of
396 Brown Carbon over the Central Indo- Gangetic Plain, , doi:10.1021/acs.est.7b00734, 2017.

397 Schmid, O., Artaxo, P., Arnott, W. P., Chand, D., Gatti, L. V., Frank, G. P., Hoffer, A.,
398 Schnaiter, M. and Andreae, M. O.: Spectral light absorption by ambient aerosols influenced by
399 biomass burning in the Amazon Basin. I: Comparison and field calibration of absorption
400 measurement techniques, *Atmos. Chem. Phys.*, 6(11), 3443–3462, doi:10.5194/acp-6-3443-2006,
401 2006.

402 Segura, S., Estellés, V., Titos, G., Lyamani, H., Utrillas, M. P., Zotter, P., Prévôt, A. S. H.,
403 Močnik, G., Alados-Arboledas, L. and Martínez-Lozano, J. A.: Determination and analysis of in
404 situ spectral aerosol optical properties by a multi-instrumental approach, *Atmos. Meas. Tech.*,
405 7(8), 2373–2387, doi:10.5194/amt-7-2373-2014, 2014.

406 Sun, H., Biedermann, L. and Bond, T. C.: Color of brown carbon : A model for ultraviolet and
407 visible light absorption by organic carbon aerosol, , 34(August), 1–5,
408 doi:10.1029/2007GL029797, 2007.

409 Tan, H., Yin, Y., Gu, X., Li, F., Chan, P. W., Xu, H., Deng, X. and Wan, Q.: An observational
410 study of the hygroscopic properties of aerosols over the Pearl River Delta region, *Atmos.*
411 *Environ.*, 77, 817–826, doi:10.1016/j.atmosenv.2013.05.049, 2013.

412 Tan, H., Liu, L., Fan, S., Li, F., Yin, Y., Cai, M. and Chan, P. W.: Aerosol optical properties and
413 mixing state of black carbon in the Pearl River Delta, China, *Atmos. Environ.*, 131, 196–208,
414 doi:10.1016/j.atmosenv.2016.02.003, 2016.

415 Wang, Y., Hu, M., Lin, P., Guo, Q., Wu, Z., Li, M., Zeng, L., Song, Y., Zeng, L., Wu, Y., Guo,
416 S., Huang, X. and He, L.: Molecular Characterization of Nitrogen-Containing Organic
417 Compounds in Humic-like Substances Emitted from Straw Residue Burning, *Environ. Sci.*
418 *Technol.*, 51(11), 5951–5961, doi:10.1021/acs.est.7b00248, 2017.

419 Washenfelder, R. A., Attwood, A. R., Brock, C. A., Guo, H., Xu, L., Weber, R. J., Ng, N. L.,
420 Allen, H. M., Ayres, B. R., Baumann, K., Cohen, R. C., Draper, D. C., Duffey, K. C., Edgerton,
421 E., Fry, J. L., Hu, W. W., Jimenez, J. L., Palm, B. B., Romer, P., Stone, E. A., Wooldridge, P. J.
422 and Brown, S. S.: Biomass burning dominates brown carbon absorption in the rural southeastern
423 United States, *Geophys. Res. Lett.*, 42(2), 653–664, doi:10.1002/2014GL062444, 2015.

424 Weingartner, E., Saathoff, H., Schnaiter, M., Streit, N., Bitnar, B. and Baltensperger, U.:
425 Absorption of light by soot particles: Determination of the absorption coefficient by means of
426 aethalometers, *J. Aerosol Sci.*, 34(10), 1445–1463, doi:10.1016/S0021-8502(03)00359-8, 2003.

427 Wu, D., Mao, J. T., Deng, X. J., Tie, X. X., Zhang, Y. H., Zeng, L. M., Li, F., Tan, H. B., Bi, X.
428 Y., Huang, X. Y., Chen, J. and Deng, T.: Black carbon aerosols and their radiative properties in
429 the Pearl River Delta region, *Sci. China, Ser. D Earth Sci.*, 52(8), 1152–1163,
430 doi:10.1007/s11430-009-0115-y, 2009.

431 Wu, D., Wu, C., Liao, B., Chen, H., Wu, M., Li, F., Tan, H., Deng, T., Li, H., Jiang, D. and Yu,
432 J. Z.: Black carbon over the South China Sea and in various continental locations in South China,
433 *Atmos. Chem. Phys.*, 13(24), 12257–12270, doi:10.5194/acp-13-12257-2013, 2013.

434 Yan, C., Zheng, M., Bosch, C., Andersson, A., Desyaterik, Y., Sullivan, A. P., Collett, J. L.,
435 Zhao, B., Wang, S., He, K. and Gustafsson, Ö.: Important fossil source contribution to brown
436 carbon in Beijing during winter, *Nat. Publ. Gr.*, 1–10, doi:10.1038/srep43182, 2017.

437 Yuan, J. F., Huang, X. F., Cao, L. M., Cui, J., Zhu, Q., Huang, C. N., Lan, Z. J. and He, L. Y.:
438 Light absorption of brown carbon aerosol in the PRD region of China, *Atmos. Chem. Phys.*,
439 16(3), 1433–1443, doi:10.5194/acp-16-1433-2016, 2016.

440 Zhu, C.-S., Cao, J.-J., Hu, T.-F., Shen, Z.-X., Tie, X.-X., Huang, H., Wang, Q.-Y., Huang, R.-J.,
441 Zhao, Z.-Z., Močnik, G. and Hansen, A. D. A.: Spectral dependence of aerosol light absorption
442 at an urban and a remote site over the Tibetan Plateau, *Sci. Total Environ.*, 590–591(97), 14–21,
443 doi:10.1016/j.scitotenv.2017.03.057, 2017.

444 Zou, Y., Deng, X. J., Zhu, D., Gong, D. C., Wang, H., Li, F., Tan, H. B., Deng, T., Mai, B. R.,
445 Liu, X. T. and Wang, B. G.: Characteristics of 1 year of observational data of VOCs, NO_x and O₃
446 at a suburban site in Guangzhou, China, *Atmos. Chem. Phys.*, 15(12), 6625–6636,
447 doi:10.5194/acp-15-6625-2015, 2015.

448

449 Table

450 Table 1. Multilinear regression analyses between b_{BrC} at each wavelength and mass loading of different OA factors from AMS-PMF/ME-
451 2.

| | 370 nm | | 470 nm | | 520 nm | | 590 nm | | 660 nm | |
|--------------|----------------------------------------|---------------------------|----------------------------------------|---------------------------|----------------------------------------|---------------------------|----------------------------------------|---------------------------|----------------------------------------|---------------------------|
| | Correlation factor ($m^2 g^{-1}$) | Contribution to b_{BrC} | Correlation factor ($m^2 g^{-1}$) | Contribution to b_{BrC} | Correlation factor ($m^2 g^{-1}$) | Contribution to b_{BrC} | Correlation factor ($m^2 g^{-1}$) | Contribution to b_{BrC} | Correlation factor ($m^2 g^{-1}$) | Contribution to b_{BrC} |
| HOA | 0.61 ± 0.05 | 22.7% | 0.38 ± 0.03 | 25.4% | 0.22 ± 0.02 | 24.5% | 0.16 ± 0.02 | 25.1% | 0.16 ± 0.01 | 27.9% |
| BBOA | 3.4 ± 0.41 | 25.2% | 1.2 ± 0.26 | 15.9% | 0.63 ± 0.18 | 13.9% | 0.43 ± 0.14 | 13.4% | 0.21 ± 0.11 | 10.3% |
| LVOOA | 1.04 ± 0.08 | 52.2% | 0.65 ± 0.05 | 58.7% | 0.41 ± 0.04 | 61.5% | 0.29 ± 0.03 | 61.5% | 0.26 ± 0.02 | 61.3% |

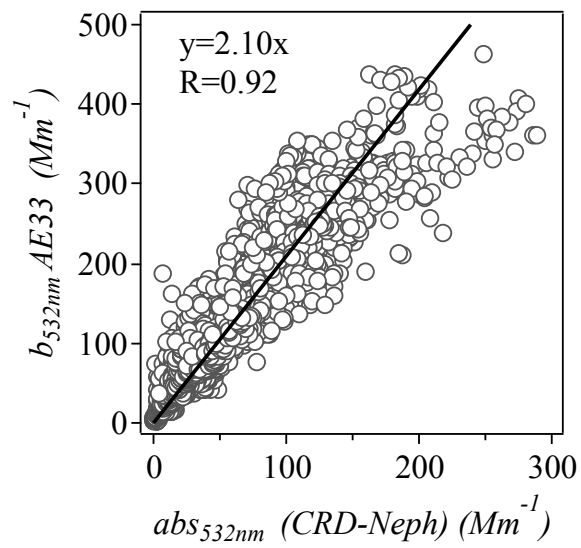
452

453 Notes: 1) Correlation coefficient (R) for each regression analysis: 0.65 at 370 nm, 0.58 at 470 nm, 0.51 at 520 nm, 0.51 at 570 nm and 0.54 at 660 nm; 2) The
454 correlation factors for COA and SVOOA are near zero at all wavelength, indicating a negligible contribution from these factors. So only the correlation factors for
455 HOA, BBOA and LVOOA are listed in the table

456

457

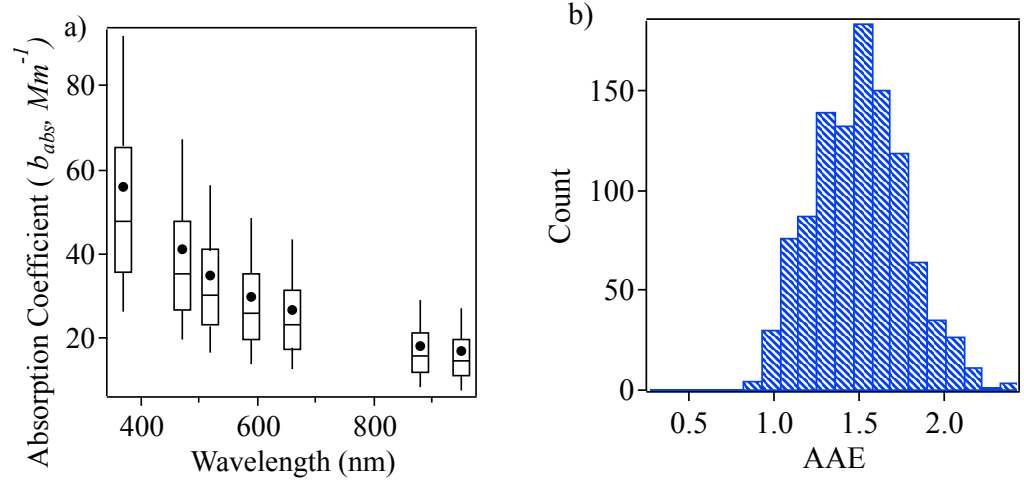
458 Figures



459

460 Figure 1. Scatter plot of absorption coefficients at 532 nm measured with aethalometer (AE33)
461 and those estimated from cavity ring-down spectroscopy (CRD) and Nephelometer measurements.

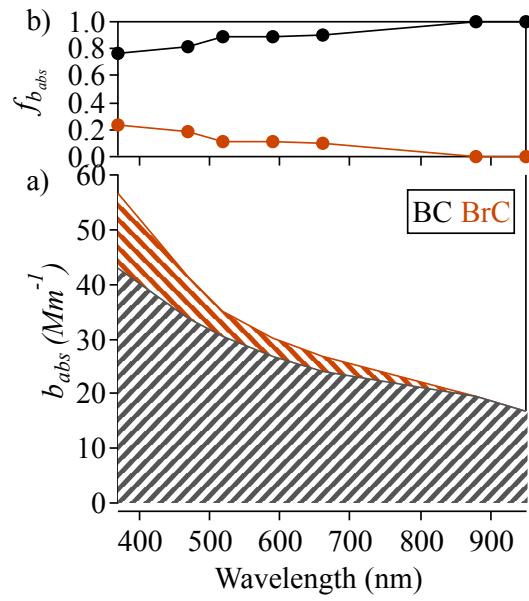
462



463

464 Figure 2. a) Box-whisker plot of absorption coefficient at seven wavelengths as measured with
 465 the AE33; b) Histogram of AAE values over the measurement campaign.

466

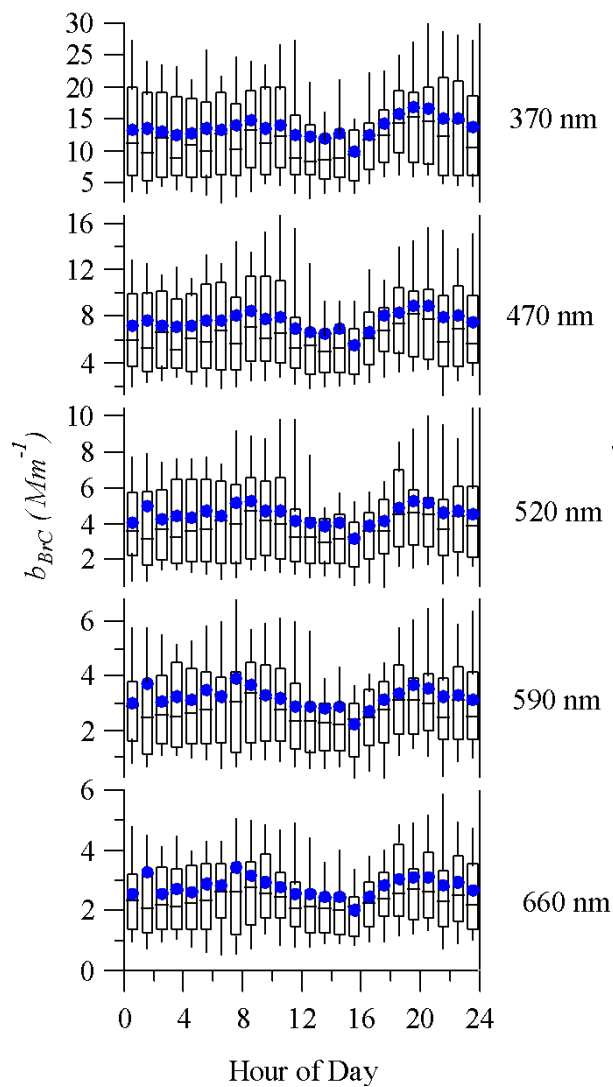


467

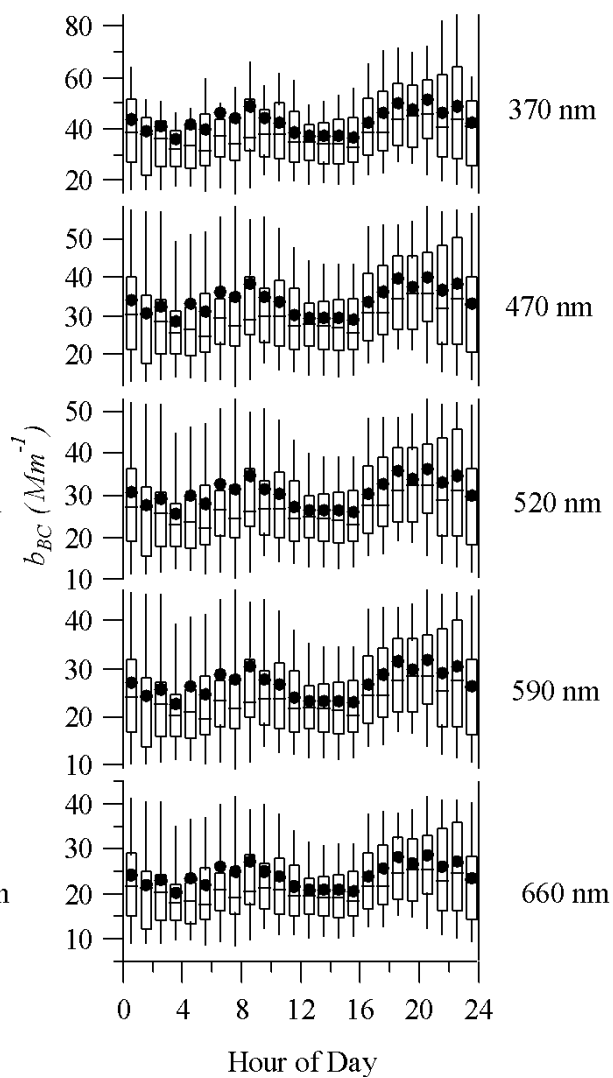
468 Figure 3. a) Fractions of BC and BrC contributions to aerosol particle light absorption at different
 469 wavelengths; b) Contributions of BC and BrC to the total light absorption coefficient at different
 470 wavelengths.

471

1) Diurnal Variations of Brown Carbon b_{BrC}



2) Diurnal Variations of Black Carbon b_{BC}

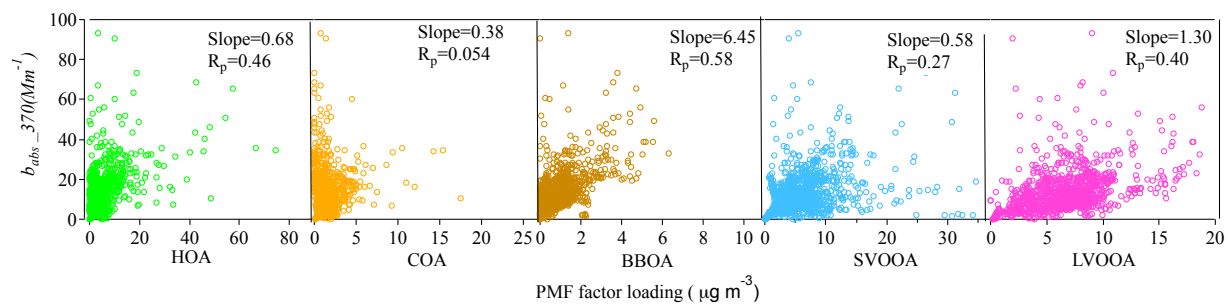


472

473 Figure 4. Diurnal variations of BrC and BC light absorption coefficients (b_{BrC} and b_{BC}) at different
474 wavelengths.

475

476



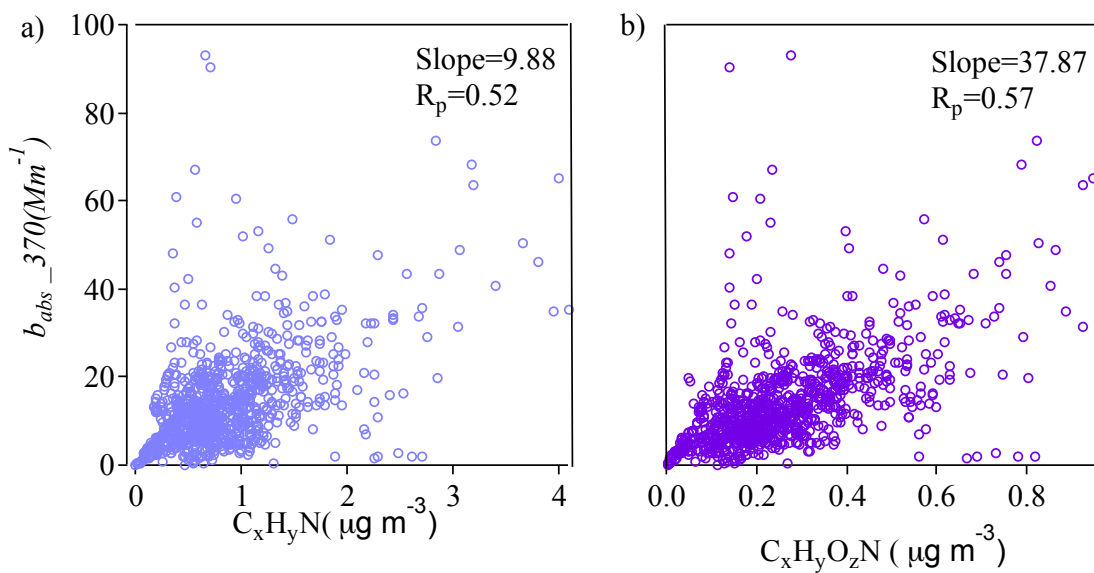
477

478 Figure 5. Correlations between the BrC absorption coefficients at 370 nm and the mass loadings
479 of OA factors resolved by AMS-PMF/ME-2.

480

481

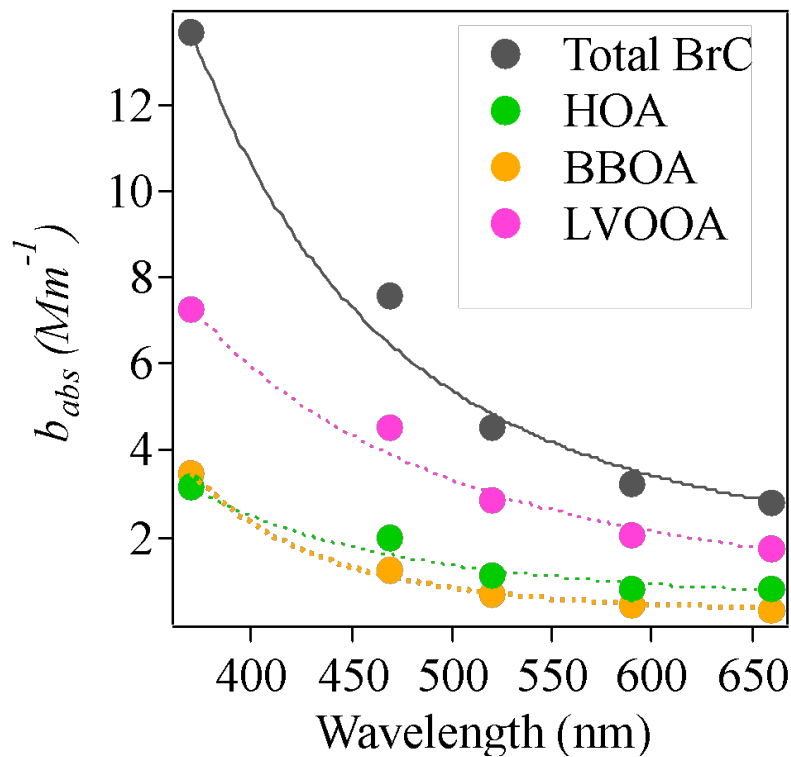
482



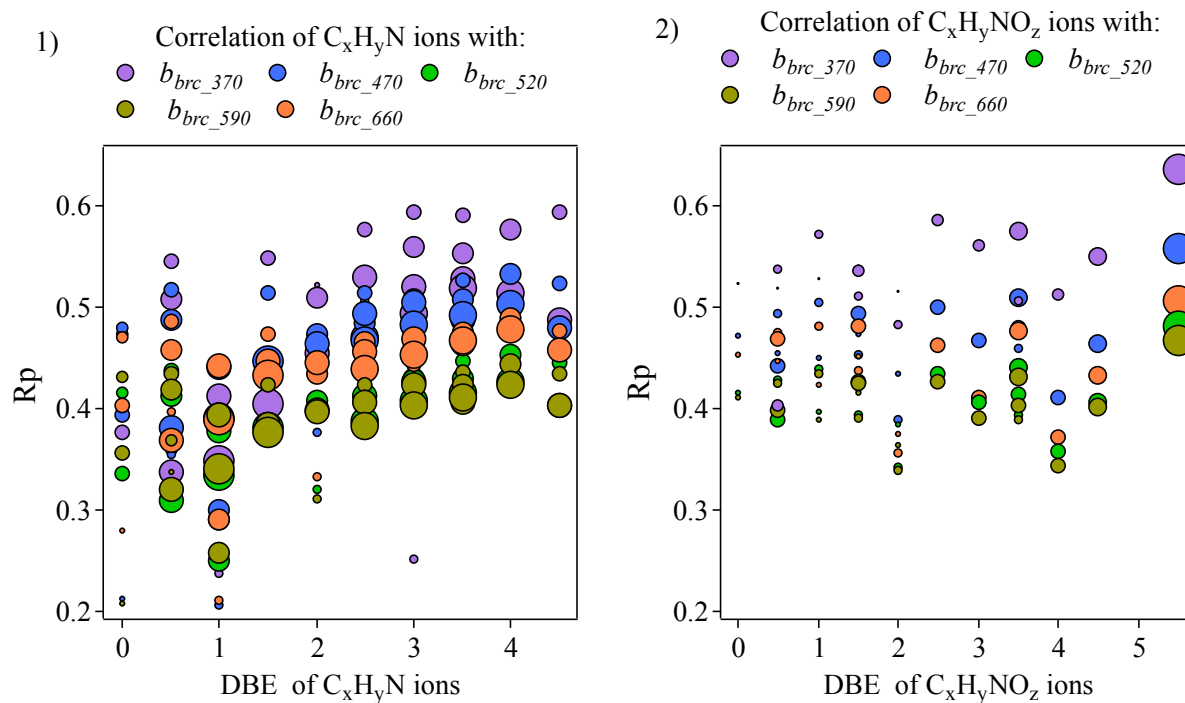
483

484 Figure 6. Correlations between BrC absorption coefficients at 370 nm and mass concentrations of
485 N-containing organic ion families.

486



487
 488 Figure 7. Exponential decay of b_{abs} for total BrC and different light-absorbing OA components
 489 across wavelength.
 490



491
 492
 493
 494
 495
 496
 497
 498
 499
 500
 24

492 Figure 8. Correlation coefficients between BrC absorption coefficient across different wavelength
493 and N-containing organic ion fragments grouped by double bond equivalence (panels a and b).
494 Larger grey dots correspond to higher carbon numbers.